Evolution of Carbon Sinks in a Changing Climate

Inez Fung*[†], Scott C. Doney[‡], Keith Lindsay[§], Jasmin John*

*Berkeley Atmospheric Sciences Center, University of California, Berkeley, Berkeley CA 94720-4767, USA. [‡] Department of Marine Chemistry and Geochemistry, Woods Hole Oceanographic Institution, Woods Hole, MA 02543 USA. [§]National Center for Atmospheric Research, P.O. Box 3000, Boulder CO 80307, USA.

[†]To whom correspondence should be addressed: Inez Fung, Berkeley Atmospheric Sciences Center, University of California, Berkeley, Berkeley CA 94720-4767, USA. Telephone: 510 643 9367. Fax: 510 643 9980. e-mail: inez@atmos.berkeley.edu.

Contributed by Inez Fung. June 13 2005

Abstract Climate change is expected to influence the capacities of the land and oceans to act as repositories for anthropogenic CO_2, and hence provide a feedback to climate change. A series of experiments with the NCAR-CSM1 coupled carbon-climate model shows that carbon sink strengths are inversely related to the rate of fossil fuel emissions, so that carbon storage capacities of the land and oceans decrease and climate warming accelerates with faster CO_2 emissions. Furthermore, there is a positive feedback between the carbon and climate systems, so that climate warming acts to increase the airborne fraction of anthropogenic CO_2 and amplify the climate change itself. Globally, the amplification is small at the end of the 21st century in this model because of its low transient climate response, and the near-cancellation between large regional changes in the hydrologic and ecosystem responses. Analysis of our results in the context of comparable models suggests that destabilization of the tropical land sink is qualitatively robust, though its degree is uncertain.

The degree of climate warming is determined by the radiative forcing and feedback processes in the climate system. Given a fossil fuel CO_2 emission, the level of CO_2 in the atmosphere, and hence the radiative forcing, is dependent on the efficiencies of the land and oceans in absorbing the excess CO_2. These efficiencies themselves change with climate and with atmospheric CO_2 levels, so that the carbon cycle represents a critical feedback mechanism in the climate system. The first 19^{th} to 21^{st} century experiments of the response of two coupled carbon-climate models to similar fossil fuel emission scenarios show that their atmospheric CO_2 level, and hence climate warming, differ dramatically by almost 200 ppmv and 2 K by 2100 (1, 2). The differences arise not only because of the different climate sensitivities of the models, but also because of the differences in land and ocean uptake characteristics and hence feedbacks between the carbon and climate systems (3).

Here we present and analyze a suite of transient experiments (1820-2100) from a new, coupled global carbon-climate model (4) developed in the framework of the National Center for Atmospheric Research (NCAR) Community Climate System Model (CCSM) (5). We focus primarily on the global carbon-climate feedbacks and the biogeochemical mechanisms that amplify or diminish physical climate change. More detailed discussion on the simulated responses of the terrestrial and oceanic carbon cycles and their sensitivity to climate and CO_2 fertilization will be presented separately.

Carbon-Climate Model and Experiments

The physical climate core of the coupled carbon-climate model is a modified version of NCAR CSM1.4, which consists of atmosphere, land, ocean and ice components that are coupled via a flux coupler (6, 7). Into CSM1.4 are embedded a modified version of the terrestrial biogeochemistry model CASA, termed CASA' (8) and a modified version of the OCMIP-2 oceanic biogeochemistry model (9, 10). The coupled carbon-climate model is summarized in Supporting Information and described in detail in (4).

CASA' follows the life cycles of plant functional types from carbon assimilation via photosynthesis, to mortality and decomposition, and the return of CO_2 to the atmosphere via microbial respiration. There are three live vegetation pools and nine soil pools, and the rates of carbon transfer among them are climate sensitive (11, 12). The carbon cycle is coupled to the water cycle via transpiration, and to the energy cycle via dynamic leaf phenology (and hence albedo). A terrestrial CO_2 fertilization effect is possible in the model because carbon assimilation via the Rubisco enzyme is limited by internal leaf CO_2 concentrations; net primary productivity (NPP) thus increases with external atmospheric CO_2 concentrations, eventually saturating at high CO_2 levels.

The ocean biogeochemical model includes in simplified form the main processes for the solubility carbon pump, organic and inorganic biological carbon pumps, and air-sea CO_2 flux. New/export production is computed prognostically as a function of light, temperature, phosphate and iron concentrations. A fully dynamic iron cycle also has been added including atmospheric dust deposition/iron dissolution, biological uptake, vertical particle transport, and scavenging.

Control experiments of CSM1 (without an interactive carbon cycle and with atmospheric CO_2 fixed at 280 ppmv) display stable surface temperatures and minimal deep ocean drift without requiring surface heat or freshwater flux adjustments. In benchmark studies, the transient climate response (TCR), i.e. temperature increase at the

time of doubling of CO_2 when climate models are forced by a 1% y^{-1} increase in CO_2, is 1.4K for the NCAR CSM1 (13).

In the fully-coupled carbon-climate model, atmospheric CO_2 is a prognostic variable and is predicted as the residual after carbon exchanges with the land and ocean. A suite of transient experiments (1820-2100) has been conducted with the resulting coupled climate-carbon cycle model, CSM 1.4-carbon (Table 1). The experiments branch off at year 100 from a stable, 1000 year pre-industrial control carbon-climate experiment (global mean annual surface temperature 13.8±0.1 deg. C; atmospheric CO_2 283±1.2 ppmv) (4). The experiments are forced by specifications of fossil fuel CO_2 emission, with historical emission trajectory for the 19th and 20th centuries (14-16) and two fossil fuel emission scenarios for 21st century: SRES-A1B, the "balanced energy sources" scenario; and SRES-A2, the "business-as-usual" scenario (17, 18). These scenarios represent high and low estimates of emissions. No other greenhouse gases or perturbations to the radiative forcing are included. For the SRES A2 emission scenario, we have carried out a pair of experiments bounding CO_2 fertilization of terrestrial photosynthesis: the biogeochemical CO_2 is set to be either the evolving CO_2 concentration in the lowest 60 mb of the atmosphere, or 280 ppmv. The global distribution of plant functional types remains time-invariant throughout all the experiments. Carbon sources associated with anthropogenic land use modification are not included in these experiments. As the other radiative forcing nearly cancel in the 19th and 20th centuries (19), the climate simulation should be broadly comparable to that observed in the globally averaged sense. However, over the 19th and 20th centuries, land-use modification accounts for approximately 35% of the cumulative anthropogenic source of atmospheric CO_2. Thus the modeled atmospheric CO_2 concentrations cannot be directly compared with that observed for a particular year.

Results

We focus our analysis on the changing carbon cycle, as the climate response to a changing CO_2 abundance in the atmosphere follows principally from the climate sensitivity of the physical climate model. We shall use the notation $\Delta\chi$ to denote a temporal change of χ in an experiment, and the notation δ to denote the departure of χ in an experiment with carbon-climate coupling from that without (ROL minus OL, or RO minus O in the notation defined in Table 1). In experiments without carbon-climate coupling, the radiative-active CO_2 is specified to be 283 ppmv, that of the control run, and the increasing CO_2 concentration forces changes in the land and ocean carbon cycles. There are small temperature changes in the experiments without radiative CO_2 carbon-climate coupling relative to the control, because of differences in albedo and evapotranspiration due to vegetative processes responding to elevated atmospheric CO_2.

Global Budgets The cumulative emission of fossil fuel CO_2 is 276 PgC for the 19th and 20th centuries, and 1380 and 1732 PgC for the 21st century for emission scenario SRES-A1B and SRES-A2, respectively. ΔCO_2 at the end of the three centuries would be 825 and 993 ppmv, for A1B and A2 scenarios respectively, if all the CO_2 remained airborne. The globally averaged changes in surface air temperature (T_{air}) and carbon budgets for the historical and 21th century experiments are summarized in Table 2.

The historical experiments for fossil fuel CO_2 emission show a reasonable simulation of the carbon budget, with globally averaged column CO_2 increasing from 282 ppmv in

1820 to ~345 ppmv with CO_2 fertilization on land (H_ROL). The simulated CO_2 is lower than that observed for 2000AD as the experiments did not include land use modification, whose cumulative emission is approximately half that of fossil fuel emission over this period. Globally averaged surface air temperature (ΔT_{air}) increases by 0.3-0.4K in H_ROL, which is barely significant statistically (one standard deviation is 0.1K in the control experiment Ctl_ROL). As can be expected from studies of the contemporary carbon cycle, the climate change over the 19th and 20th century is too small to significantly impact the carbon cycle, so that the partitioning of carbon among the atmosphere, land and ocean reservoirs is approximately the same with and without carbon-climate coupling, with the airborne fraction hovering around 50% with a CO_2 fertilization sink on land.

In experiments H_RO and H_O, there is no land sink for fossil fuel CO_2. Both the oceans and the atmosphere increase their fossil fuel fractions, and ΔT_{air} increases accordingly. The airborne fraction of 70% without a land sink is higher than is observed for this period.

Figure 1 shows the evolution, versus global mean atmospheric CO_2 concentration, of f_{land} and f_{ocn}, the cumulative land and ocean carbon sinks expressed as fractions of the cumulative emission for the three pairs of experiments: A1B_ROL and A1B_OL; A2_ROL and A2_RO; and A2_RO and A2_O. Fossil fuel emission in SRES scenario A1B increases until 2050AD and decreases thereafter, while that in A2 increases exponentially over the period. With increasing rates of emission in A2, carbon sequestration processes on land and in the ocean cannot keep up with the emissions, as they have longer time constants than the emission. Furthermore, the capacities of the sinks diminish with increasing CO_2, so that both f_{land} and f_{ocn} decrease with increasing CO_2 in the atmosphere. The A1B emission rate is slower in comparison, so that the mixing of excess of carbon into the deep ocean can maintain a surface ocean CO_2 partial pressure (pCO_2) increase that is slower than that in the atmosphere, and f_{ocn} steadily increases.

Table 2 shows the bulk sink fractions for the experiments for the historical period and for the 21st century. With the land sink operating, f_{land} is ~30% in the historical experiments for the 19th and 20th centuries, and ~28% in the A1B experiments and ~25% in the A2 experiments for 21st century, showing that the land sink cannot catch up with the fossil fuel emissions, even in this hypothetical case with no nutrient and other limitations on CO_2 fertilization. In the A1B experiments, the oceans partially make up for the reduced land uptake, so that the airborne fractions ($=1 - f_{land} - f_{ocn}$) are similar to those in the historical experiments (46-48%). In the A2 experiments with or without carbon-climate coupling, the oceans actually decrease, albeit by only ~1%, their uptake fraction in the 21st century compared to the historical period: the higher rate of CO_2 increase in the atmosphere is not matched by the rate of excess CO_2 removal out of the mixed layer. As a result of the reduced land and ocean uptake fractions, the airborne fraction in the 21st century (52-54%) is higher with the higher fossil fuel emission than that in the 19th and 20th centuries (46-48%). In experiments without the land sink (A2_RO and A2_O), f_{ocn} is higher than that in experiments with the land sink (A2_ROL and A2_O) because of the higher CO_2 in the atmosphere.

Contrary to results from similar coupled carbon-climate experiments (1, 2, 20-22), this model yields only a very small difference in global carbon budgets (δCO_2 ~15-20

ppmv) whether carbon-climate coupling is included or not. Both f_{land} and f_{ocn} are reduced with carbon-climate coupling, though δf_{land} and δf_{ocn} are small ~ –1-2%. The causes for relatively constant partitioning of anthropogenic CO_2 with and without carbon-climate coupling are investigated in detail below.

Ocean Carbon Sink Greenhouse warming influences the oceanic carbon cycle indirectly through changes in ocean circulation and air-sea exchange of CO_2. The magnitude of the ocean carbon sink is dependent on several competing effects on the CO_2 partial pressure difference across the air-sea interface. Warming reduces solubility and increases pCO2 in the mixed layer. Warming (and freshening) increase ocean stratification, reduce vertical mixing, and slow the thermohaline circulation, leading to slower removal of excess carbon from the surface ocean. Increased stratification reduces the delivery of nutrients and inorganic carbon to the euphotic zone in most regions, and lowers biological productivity. The resultant pCO_2 in the mixed layer decreases if the reduction in carbon supply exceeds the reduction in biological consumption and export. The accumulation of CO_2 in the ocean decreases pH and shifts carbonate chemistry to higher dissolved CO_2 gas fractions. Finally, for the same fossil fuel emission, atmospheric CO_2 levels and air-sea pCO2 difference increase if the land carbon sink decreases.

In A2_ROL, sea surface temperature at year 2100 is higher by 1.2K; North Atlantic overturning is slower by 17%; and the export carbon flux is smaller by 5% compared to A2_OL. Their combined effects on ocean carbon uptake is shown in Figure 2a, the difference in the column inventory of total inorganic carbon near the end of the 21st century between experiment A2_ROL and A2_OL at atmospheric CO_2 concentration of 765 ppmv (2094-2098AD in A2_ROL and 2096-2100AD in A2_OL). Globally the cumulative inventory in excess carbon in Figure 2a is lower by ~20 PgC in A2_ROL relative to A2_OL. Circulation effects are most evident in the lower carbon inventory in the subpolar/polar North Atlantic but reductions occur also in the tropical north Indo-Pacific, and Southern Ocean and Antarctic coast, where excess CO_2 enters the oceans, and in the western Atlantic along the path of North Atlantic Deep Water. In the temperate Northern Hemisphere, declines in the upward transport of carbon and nutrients to the surface layer lead to reduced biological production and surface phosphate (not shown); the net biological effect is to lower surface pCO_2 and increase ocean uptake, thus partially compensating for the slower physical circulation. Integrated production in the Southern Ocean remains about the same, though it tends to shift poleward due to a change in ocean upwelling patterns.

Land Carbon Sink The cumulative land sinks in the transient experiments result from the differing sensitivities of net primary productivity (NPP) and respiration to changes in CO_2, light, temperature and moisture regimes, and their competitive effects on carbon inventory in vegetation and soils. In general, warming and moistening would accelerate NPP and vegetation biomass, and shorten the turnover time of soils.

For both A1B and A2 emission scenarios, the CO_2 fertilization sink on land is only slightly lower, by ~20 PgC, in the experiments with carbon-climate coupling than in those without (Table 2). For experiments without CO_2 fertilization (A2_RO and A2_O), the land acts as a small net source to the atmosphere with carbon-climate coupling. This result is very different from those of other similar models (1-3, 21, 22), in which climate

feedbacks lead to massive destabilization of the land sink. Here we focus on the experiments with the higher emission scenario (A2) and hence greater potential for carbon-climate feedback. Experiment A2_OL shows a cumulative net flux (or biomass increase) of 445 PgC into the biosphere in the 21st century, as there is CO_2 fertilization. The effect of carbon-climate coupling on the land sink is shown as δBiomass (sum of vegetation and soil carbon pools) at an atmospheric CO_2 concentration of 765 ppmv (Figure 2b). Compared with A2_OL, A2_ROL has less uptake in the tropics and greater uptake in high latitudes, so that globally there is little change between the two experiments.

Soil moisture is the difference between precipitation and temperature-dependent evapotranspiration. With warm climates, the demand for moisture exceeds the supply even though there may be an increase in rainfall, so that there is a tendency in the model for warming to lead to drier regimes in warm regions (tropics, summer) and to wetter regimes in cold regions (Figure 3a). The consequence of these differing hydrologic regimes is seen in Figure 3b, the regression of annual mean δ*NPP* against annual mean $\delta T_{air.}$ At low latitudes, the regression coefficient is negative; i.e., NPP is lower in the warmer world because of soil dessication. At middle to high latitudes, NPP is higher in A2_ROL compared to A2_OL because of more favorable climate. The effects of decreased NPP in the tropics lead to smaller vegetation and soil carbon pools, which, when combined with the faster decomposition rate, yield lower carbon storage. Thus there is local competition between temperature and moisture in determining the carbon source/sink strength, with significant regional cancellation in net carbon storage between the tropics and high latitudes.

Discussion and Summary

Experiments with the carbon-climate model NCAR CSM1 show that the land and oceans decrease their capacity to act as repositories of fossil fuel CO_2 as fossil fuel CO_2 emissions accelerate and greenhouse warming progresses. In terms of global budgets, the model yields minimal difference between experiments with and without carbon-climate coupling, compared with δCO_2 of 280 and 80 ppmv for the Hadley Centre model (1) and IPSL model (2), respectively, because of the weaker carbon-climate coupling in the NCAR CSM1. To begin with, the transient climate response (TCR) is 1.4K for NCAR CSM1 (13), at the low end of the range 1.1-3.1K for climate models (18). The magnitude of the ocean carbon sink to carbon-climate feedbacks depends on the representation of ocean circulation in the physical climate model (23, 24) and its response to changing climate, as well as on the sensitivity of marine ecosystem processes to the changing ocean climate (25, 26). The NCAR CSM1 has a stronger fossil fuel CO_2 uptake (and a lower airborne CO_2 fraction) with the control climate than, for example, the Hadley model, and this sets the stage for weaker coupling between the carbon-climate systems.

The magnitude of the land carbon sink and its response to carbon-climate feedbacks depend on the turnover times of the carbon pools, the sensitivity of terrestrial processes to climate change, as well as on the transient climate and hydrologic response of the physical climate model. The turnover time of vegetation and soil carbon, or the lag between photosynthesis and respiration, determines to the lowest order, the magnitude of the carbon sink itself. TRIFFID, the dynamic vegetation model in (1), whose single soil carbon pool has a turnover time of 25 years, thus has potentially a greater carbon storage

capacity than CASA', which has 9 soil carbon pools and a turnover time of <5 years for ~60% of the soil carbon. The shorter turnover time is consistent with flux-weighted times derived from ^{14}C measurements (27). Intercomparison of six ecosystem models shows that TRIFFID also has the steepest photosynthesis and respiration increase in response to specified 19th to 21st century climate change and CO_2 increase (28). Multiplying this high ecosystem sensitivity is the high TCR (3.5K) of the climate model HadCM3, so that the coupled carbon-climate model yields, by 2050, tropical temperatures above the optimal temperature for photosynthesis. The excess heating drives the dieback of the rainforest, accelerates soil carbon loss, and transforms the land from a sink to a source of carbon for the atmosphere (29). In the IPSL model, with an intermediate TCR of ~2K, the reduction in photosynthesis due to warming and drying in the tropics exceeds the increase in photosynthesis due to lengthening of the growing season at high latitudes, so that there is a net reduction in the strength of the global land sink (30). In the NCAR CSM1, the climate and ecosystem changes are qualitatively similar to that in the IPSL model. However, with the low TCR of 1.4K, the decrease in carbon sink at low latitudes nearly cancels the increase at high latitude, with little change in the global net land sink in the NCAR CSM1. The temperature increases are below the threshold values for vegetation dieback.

While there are observations of precipitation trends, there is a paucity of observations of soil moisture, especially in the tropics, to permit quantification of the competitive and/or synergistic effects of temperature and hydrologic changes on photosynthesis and respiration. Satellite and site data also show that interannual and interdecadal variations in biological productivity are sensitive to variations in the hydrologic regime as well as to variations in temperature (31-36). And so the increasing destabilization of the terrestrial carbon sink with warming and drying as modeled by coupled carbon-climate models such as presented here is qualitatively plausible, even though the timing is uncertain. The timing would also depend, *inter alia*, on other climate forcing and processes not included here, e.g. dynamic vegetation, high-latitude peatlands, and ocean acidification.

Acknowledgement

We gratefully acknowledge the support and assistance provided by the NCAR Community Climate System Model Team, in particular J. Kiehl, W. Collins, G. Bonan, P. Gent, and P. Rasch. Ed Sarachik provided critical comments on the manuscript. Computations were carried out at NCAR and at NERSC. This work has been supported by the National Science Foundation grant NSF ATM-9987457, NASA EOS-IDS grant NAG5-9514, NASA Carbon Cycle Program grant NAG5-11200, Lawrence Berkeley National Laboratory LDRD, and the WHOI Ocean and Climate Change Institute. The National Center for Atmospheric Research is sponsored by the US National Science Foundation. WHOI contribution 11389.

References

1. Cox, P. M., Betts, R. A., Jones, C. D., Spall, S. A. & Totterdell, I. J. (2000) *Nature* 408, 184-187.
2. Dufresne, J. L., Friedlingstein, P., Berthelot, M., Bopp, L., Ciais, P., Fairhead, L., Le Treut, H. & Monfray, P. (2002) *Geophysical Research Letters* 29.

3. Friedlingstein, P., Dufresne, J. L., Cox, P. M. & Rayner, P. (2003) *Tellus Series B-Chemical and Physical Meteorology* 55, 692-700.
4. Doney, S. C., Llindsay, K., Fung, I. & John, J. (2005) *J. Climate*, to be submitted.
5. Blackmon, M., Boville, B., Bryan, F., Dickinson, R., Gent, P., Kiehl, J., Moritz, R., Randall, D., Shukla, J., Solomon, S., Bonan, G., Doney, S., Fung, I., Hack, J., Hunke, E., Hurrell, J., Kutzbach, J., Meehl, J., Otto-Bliesner, B., Saravanan, R., Schneider, E. K., Sloan, L., Spall, M., Taylor, K., Tribbia, J. & Washington, W. (2001) *Bulletin of the American Meteorological Society* 82, 2357-2376.
6. Boville, B. A., Kiehl, J. T., Rasch, P. J. & Bryan, F. O. (2001) *Journal of Climate* 14, 164-179.
7. Boville, B. A. & Gent, P. R. (1998) *Journal of Climate* 11, 1115-1130.
8. Randerson, J. T., Thompson, M. V., Conway, T. J., Fung, I. Y. & Field, C. B. (1997) *Global Biogeochemical Cycles* 11, 535-560.
9. Doney, S. C., Lindsay, K. & Moore, J. K. (2003) Ocean Biogeochemistry: The role of the ocean carbon cycle in global change, ed: M.J.R. Fasham, Springer-Verlag, , 217-238.
10. Najjar, R., Sarmiento, J. & Toggweiler, J. R. (1992) *Global Biogeochemical Cycles* 6, 45-76.
11. Dickinson, R. E., Shaikh, M., Bryant, R. & Graumlich, L. (1998) *Journal of Climate* 11, 2823-2836.
12. Friedlingstein, P., Joel, G., Field, C. B. & Fung, I. Y. (1999) *Global Change Biology* 5, 755-770.
13. Meehl, G.A., Collins, W.D., Boville, B., Kiehl, J.T., Wigley, T.M.L., & Arblaster, J.M. (2000) *J Climate*, 13, 1879-1898.
14. Andres, R. J., Fielding, D. J., Marland, G., Boden, T. A., Kumar, N. & Kearney, A. T. (1999) *Tellus Series B-Chemical and Physical Meteorology* 51, 759-765.
15. Marland, G. & Rotty, R. M. (1984) *Tellus Series B-Chemical and Physical Meteorology* 36, 232-261.
16. Andres, R. J., Marland, G., Fung, I. & Matthews, E. (1996) *Global Biogeochemical Cycles* 10, 419-429.
17. Nakicenovic, N., Alcamo, J., Davis, G., de Vries, B., Fenhann, J., Gaffin, S., Gregory, K., Grubler, A., Yong Jung, T., Kram, T., Lebre La Rovere, E., Michaelis, L., Mori, S., Morita, T., Pepper, W., Pitcher, H., Price, L., Riahi, K., Roehrl, A., Rogner, H.-H., Sankovski, A., Schlesinger, M., Shukla, P., Smith, S., Swart, R., van Rooijen, S., Victor, N. & Dadi, Z. (2000) *Cambridge University Press*, 500 pp.
18. *Climate Change 2001: Synthesis Report*. (Cambridge, Cambridge), 398 pp.
19. Hansen, J., Sato, M., Nazarenko, L., Ruedy, R., Lacis, A., Koch, D., Tegen, I., Hall, T., Shindell, D., Santer, B., Stone, P., Novakov, T., Thomason, L., Wang, R., Wang, Y., Jacob, D., Hollandsworth, S., Bishop, L., Logan, J., Thompson, A., Stolarski, R., Lean, J., Willson, R., Levitus, S., Antonov, J., Rayner, N., Parker, D. & Christy, J. (2002) *Journal of Geophysical Research-Atmospheres* 107.
20. Zeng, N., Qian, H. F., Munoz, E. & Iacono, R. (2004) *Geophysical Research Letters* 31.
21. Thompson, S. L., Govindasamy, B., Mirin, A., Caldeira, K., Delire, C., Milovich, J., Wickett, M. & Erickson, D. (2004) *Geophysical Research Letters* 31.

22. Govindasamy, B., Thompson, S., Mirin, A., Wickett, M., Caldeira, K. & Delire, C. (2005) *Tellus Series B-Chemical and Physical Meteorology* 57, 153-163.
23. Matsumoto, K., Sarmiento, J. L., Key, R. M., Aumont, O., Bullister, J. L., Caldeira, K., Campin, J. M., Doney, S. C., Drange, H., Dutay, J. C., Follows, M., Gao, Y., Gnanadesikan, A., Gruber, N., Ishida, A., Joos, F., Lindsay, K., Maier-Reimer, E., Marshall, J. C., Matear, R. J., Monfray, P., Mouchet, A., Najjar, R., Plattner, G. K., Schlitzer, R., Slater, R., Swathi, P. S., Totterdell, I. J., Weirig, M. F., Yamanaka, Y., Yool, A. & Orr, J. C. (2004) *Geophysical Research Letters* 31.
24. Doney, S. C., Lindsay, K., Caldeira, K., Campin, J. M., Drange, H., Dutay, J. C., Follows, M., Gao, Y., Gnanadesikan, A., Gruber, N., Ishida, A., Joos, F., Madec, G., Maier-Reimer, E., Marshall, J. C., Matear, R. J., Monfray, P., Mouchet, A., Najjar, R., Orr, J. C., Plattner, G. K., Sarmiento, J., Schlitzer, R., Slater, R., Totterdell, I. J., Weirig, M. F., Yamanaka, Y. & Yool, A. (2004) *Global Biogeochemical Cycles* 18.
25. Sarmiento, J. L., Slater, R., Barber, R., Bopp, L., Doney, S. C., Hirst, A. C., Kleypas, J., Matear, R., Mikolajewicz, U., Monfray, P., Soldatov, V., Spall, S. A. & Stouffer, R. (2004) *Global Biogeochemical Cycles* 18.
26. Lefevre, N., Watson, A. J., Olsen, A., Rios, A. F., Perez, F. F. & Johannessen, T. (2004) *Geophysical Research Letters* 31.
27. Trumbore, S. (2000) *Ecological Applications* 10, 399-411.
28. Cramer, W., Bondeau, A., Woodward, F. I., Prentice, I. C., Betts, R. A., Brovkin, V., Cox, P. M., Fisher, V., Foley, J. A., Friend, A. D., Kucharik, C., Lomas, M. R., Ramankutty, N., Sitch, S., Smith, B., White, A. & Young-Molling, C. (2001) *Global Change Biology* 7, 357-373.
29. Cox, P. M., Betts, R. A., Collins, M., Harris, P. P., Huntingford, C. & Jones, C. D. (2004) *Theoretical and Applied Climatology* 78, 137-156.
30. Berthelot, M., Friedlingstein, P., Ciais, P., Monfray, P., Dufresne, J. L., Le Treut, H. & Fairhead, L. (2002) *Global Biogeochemical Cycles* 16.
31. Angert, A., Tucker, C. J., Biraud, S., Bonfils, C., Henning, C. C., Buermann, W. & Fung, I. (2005) *Proceedings of the National Academy of Sciences of the United States of America* in press.
32. Bonfils, C., Angert, A., Henning, C., Biraud, S., Doney, S. C. & Fung, I. (2005) *Geophysical Research Letters* 32, doi:10.1029/2005GL22583.
33. Nemani, R., White, M., Thornton, P., Nishida, K., Reddy, S., Jenkins, J. & Running, S. (2002) *Geophysical Research Letters* 29.
34. Nemani, R. R., Keeling, C. D., Hashimoto, H., Jolly, W. M., Piper, S. C., Tucker, C. J., Myneni, R. B. & Running, S. W. (2003) *Science* 300, 1560-1563.
35. Huxman, T. E., Smith, M. D., Fay, P. A., Knapp, A. K., Shaw, M. R., Loik, M. E., Smith, S. D., Tissue, D. T., Zak, J. C., Weltzin, J. F., Pockman, W. T., Sala, O. E., Haddad, B. M., Harte, J., Koch, G. W., Schwinning, S., Small, E. E. & Williams, D. G. (2004) *Nature* 429, 651-654.
36. Weltzin, J. F., Loik, M. E., Schwinning, S., Williams, D. G., Fay, P. A., Haddad, B. M., Harte, J., Huxman, T. E., Knapp, A. K., Lin, G. H., Pockman, W. T., Shaw, M. R., Small, E. E., Smith, M. D., Smith, S. D., Tissue, D. T. & Zak, J. C. (2003) *Bioscience* 53, 941-952.

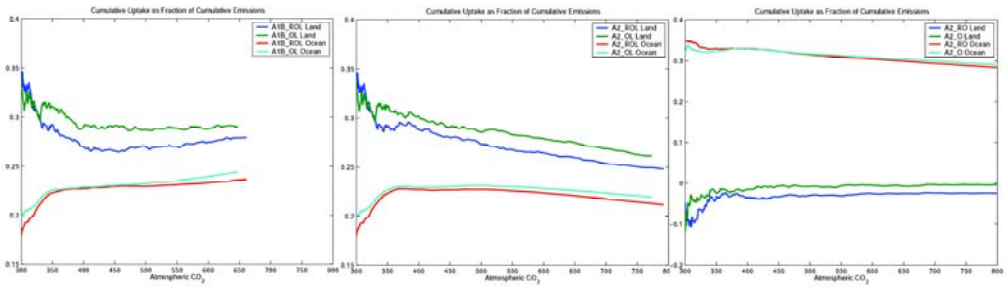

Figure 1: Evolution of f_{land} and f_{ocn}, the cumulative land and ocean sinks expressed as fractions of the cumulative emission, plotted against atmospheric CO_2 (in ppmv) for experiments (a) A1B_ROL and A1B_OL, (b) A2_ROL and A2_OL; and (c) A2_RO and A2_O.

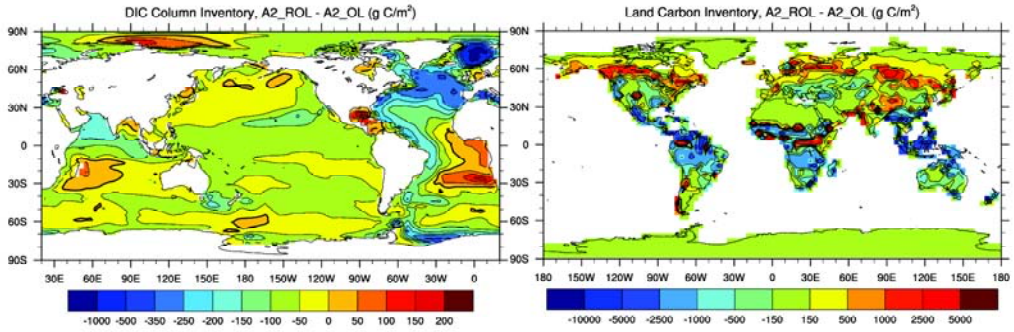

Figure 2. (a) Difference in column inventory of dissolved inorganic carbon between experiments A2_ROL and A2_OL due to effects of changing ocean circulation and ocean biogeochemistry. The inventories are averaged over times when the atmospheric CO_2 mixing ratio is 765 ppmv, i.e. 2094-2098AD in A2_ROL and 2096-2100 in A2_OL. (b) Like (a), but for terrestrial carbon inventory. Unit is gC/m^2.

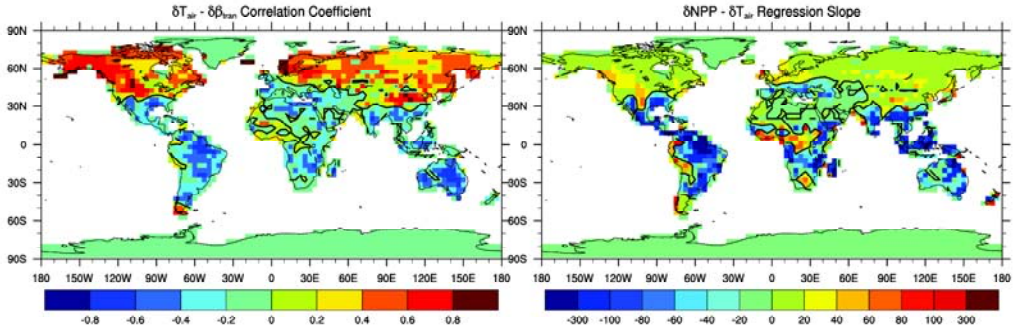

Figure 3. (a) Correlation between annual mean δT_{air} and $\delta\beta_{tran}$ for the 21st century. β_{tran} is an index (between 0 and 1) of soil moisture saturation. (b) Regression (in kg $C/m^2/K$) of annual mean δNPP against annual mean δT_{air}. δ is defined as the difference between experiments A2_ROL and A2_OL for the 21st century.

Table 1. Summary of experiments with the NCAR carbon-CSM1. Experiments are designated with the prefix "Ctl" for the control, "H" for the historical fossil fuel emissions for the 19th and 20th centuries, and "A1B" or "A2" for the SRES fossil fuel emission scenarios for the 21st century. The suffix *R* denote that radiative CO_2 in the atmosphere is given by the column average of the atmospheric CO_2 resulting from the interactive carbon cycle; and the suffices *L, O* denote that the land and ocean carbon cycles are forced by the evolving CO_2 in the lowest 60mb of the atmosphere.

Experiment	Fossil Fuel Emission	Radiative CO_2	CO_2 for Land Photosynthesis	CO_2 for Air-sea Exchange	Carbon-climate Coupling
Ctl_ROL	None	Prognostic	Prognostic	Prognostic	Yes
H_ROL	Historical	Prognostic	Prognostic	Prognostic	Yes
H_OL	Historical	283 ppmv	Prognostic	Prognostic	-
H_RO	Historical	Prognostic	280 ppmv	Prognostic	Yes
H_O	Historical	283 ppmv	280 ppmv	Prognostic	-
A1B_ROL	SRES A1B	Prognostic	Prognostic	Prognostic	Yes
A1B_OL	SRES A1B	283 ppmv	Prognostic	Prognostic	-
A2_ROL	SRES A2	Prognostic	Prognostic	Prognostic	Yes
A2_OL	SRES A2	283 ppmv	Prognostic	Prognostic	-
A2_RO	SRES A2	Prognostic	280 ppmv	Prognostic	Yes
A2_O	SRES A2	283 ppmv	280 ppmv	Prognostic	-

Table 2: Cumulative carbon budgets for the 19th to 21th centuries. Cumulative fossil fuel emission is 276 PgC for the 19th and 20th centuries. Cumulative fossil fuel emission for the 21st century is 1380 PgC and 1732 PgC for SRES A1B and SRES A2, respectively. ΔT (column 2) is the difference in global 5-year mean surface air temperature between the end of the period and the beginning of the period.

Experiment	ΔT (K)	Atmospheric CO_2 at end of period (ppmv)	Airborne fraction (%)	Land fraction (%)	Ocean fraction (%)
	1820 – 2000 AD				
H_ROL	0.35	345	49	29	22
H_OL	(0.18)*	343	47	31	22
H_RO	0.48	373	70	-3	33
H_O	(0.06)*	372	69	-2	33
	2001– 2100 AD				
A1B_ROL	1.21	661	48	28	24
A1B_OL	-0.12	647	47	29	24
A2_ROL	1.42	792	54	25	21
A2_OL	0.12	773	52	26	22
A2_RO	1.79	997	76	-2	26
A2_O	-0.13	970	73	0	27

* not statistically significant. 1σ=0.1K from Ctl_ROL.

Supporting Information

The resolution of the atmosphere model is T31 (~3.6^o) in the horizontal with 10 levels in the troposphere and 8 levels in the stratosphere. The land module has the same horizontal resolution as the atmosphere. The ocean and sea-ice modules have a horizontal resolution of 3.6^o in longitude and 0.8-1.8^o in latitude (T31x3). There are 25 vertical levels extending through the full depth of the ocean. The water cycle is closed through a river runoff scheme, and modifications have been made to the ocean horizontal and vertical diffusivities and viscosities from the original version (CSM 1.0) to improve the equatorial ocean circulation and interannual variability. The 3-D atmospheric CO_2 distribution is advected and mixed as a dry-air mixing ratio using a semi-Lagrangian scheme, and the model CO_2 field affects the shortwave and longwave radiative fluxes through the column average CO_2 concentration.

Globally, there are 14 plant functional types (PFT), with fractional coverage of up to 4 PFT's within each model gridbox. Gross primary productivity (GPP) is the canopy integral of carbon assimilation, calculated as the optimal carbon assimilation to minimize transpiration loss of water for ambient light, temperature, moisture and Vmax conditions. CASA' assumes 50% of the GPP is lost to autotrophic respiration, and tracks the carbon flow through 3 vegetation carbon pools and 9 soil carbon pools, with the flow rates modulated by climate.

To facilitate analysis of the model, we have separated atmospheric CO_2 into three "species": tracer CO_2 (C_{tracer}), which is radiatively inert, and is the three-dimensional signature of the variations in the sources and sinks; biogeochemical CO_2 (C_{BGC}), which is C_{tracer} averaged over the lowest two layers of the atmospheric model (~60 mb) and which is the CO_2 forcing for terrestrial photosynthesis and for air-sea CO_2 exchange; and radiative CO_2 (C_{rad}), which is the value of CO_2 used in the atmospheric radiation computations. With carbon-climate coupling, C_{rad} is the column average of C_{tracer}.